Interaction response of maglev masses moving on a suspended beam shaken by horizontal ground motion

J.D. Yau *

Department of Architecture, Tamkang University, Taipei 10620, Taiwan, ROC

ARTICLE INFO

ABSTRACT

As a maglev transport route has to cross a region with occasional earthquakes, the train/ guideway interaction is an issue of great concern in dominating safety of the maglev system. This paper intends to present a computational framework of interaction analysis for a maglev train traveling over a suspension bridge shaken by horizontal earthquakes. The suspended guideway girder is modeled as a single-span suspended beam and the maglev train traveling over it as a series of maglev masses. Due to *motion-dependent nature* of magnetic forces in a maglev suspension system, appropriate adjustments of the magnetic forces between magnets and guide-rail require the air gaps be continuously monitored. Thus an on-board hybrid LQR+PID controller with constraint rule base is designed to control the dynamic response of a running maglev mass. Then the governing equations of motion for the suspended beam associated with all the controlled maglev masses are transformed into a set of generalized equations by Galerkin's method, and solved using an incremental-iterative procedure. Numerical investigations demonstrate that when a controlled maglev train travels over a suspended guideway shaken by horizontal earthquakes, the proposed hybrid controller has the ability to adjust the levitation gaps in a prescribed stable region for safety reasons and to reduce the vehicle's acceleration response for ride quality.

1. Introduction

Magnetic levitation (Maglev) features the vanguard of technological advance in high speed ground transport for no physical contact with guideway and efficient energy consumption in reducing greenhouse gas emission. There are two types of maglev technologies being developed and brought to the stage of commercial (pre-commercial) demonstration: (1) the electromagnetic suspension (EMS) with attractive mode; (2) the electro-dynamic suspension (EDS) with repulsive mode [1–4]. The EMS system can lift up a train using attractive forces by the magnets beneath a guide-rail at any speed. The EDS system uses magnetic repulsive forces to suspend a train in a U-shaped guideway. One feature of an EDS-type maglev train is that its discrete maglev suspension systems [6] are workable only at high speeds with *large* guideway clearances of 0.1–0.15 m [2], which is the major difference from the EMS system. Thus the EDS-repulsive system has a larger levitation gap to accommodate additional vertical motion of the magnet due to ground motion experienced in an earthquake-prone territory.

In the last decade, a great portion of the studies on maglev dynamics is focused on the vibration of a maglev vehicle running on a flexible guideway system [5–11]. Cai and Chen [5] provided a literature review for various aspects of the

---

* Corresponding author. Tel.: +886 2 26215656×3139; fax: +886 2 23959041.
  E-mail address: jdyau@mail.tku.edu.tw

dynamic characteristics, magnetic suspension systems, vehicle stability, and suspension control laws of maglev/guideway coupling systems. Concerning the interaction response of a maglev train traveling over a flexible guideway girder, Cai et al. [6] pointed out that a concentrated-load vehicle model would result in larger response on the vehicle/guideway system than a distributed-load one. Zheng et al. [7,8] developed two kinds of vehicle/guideway coupling models with controllable magnetic suspension systems to observe the phenomena of divergence, flutter, and collision on the dynamic stability of a maglev vehicle traveling on a flexible guideway. Zhao and Zhai [9] simulated a TR06 carriage as a ten-degree-of-freedom (10-dof) rigid vehicle model to investigate the ride quality of a maglev vehicle traveling on elevated guideways. In the latest study, Yau [10,11] proposed an on-board PI controller to control the interaction response of a maglev vehicle running on flexible guideways by using an incremental-iterative procedure. However, rather limited research works seem available to conduct the influence of seismic ground motion on interaction behavior of a maglev train crossing a suspended guideway.

A suspension bridge is usually used to cross a deep valley or wide chasm [12] for its lightweight and large span. For vibration analysis of suspension bridges [13–17], an analytical model based on *linearized* deflection theory [12,13,18] was adopted to formulate the governing equations of motion for a single-span suspended beam. From the research results, one of the key findings revealed that the cable tensions of *short* or *medium span* suspension bridges would be amplified significantly when subjected to moving loads [14].

Concerning the stability problem of a train moving on a bridge shaken by earthquakes, Yang et al.'s book [19] pointed out that the presence of vertical ground excitations would affect drastically the stability of the train, especially for near resonant excitations. Xia et al. [20] revealed that seismic traveling wave effect would play an impact role in assessing the running safety of a train traveling over continuous viaducts during earthquakes. Yau and Fryba [12] indicated that vertical ground support motion would totally amplify the dynamic response of a single-span bridge subject to multiple moving loads. Generally speaking, the dynamic interaction behavior of maglev vehicle/bridge system shaken by earthquakes is of a rather complicated interaction problem involving control of magnetic forces, monitoring of levitation gaps, and multiple support motions [12,21].

The objective of this study is to present a computational framework of interaction analysis using an incremental-iterative procedure to compute the dynamic response of a *controlled* maglev train traveling over a suspended guideway shaken by horizontal earthquakes. Control of levitation forces between the magnet and guide-rail requires the guideway clearance be continuously monitored. Thus a hybrid LQR+PID controller is designed to meet the performance criteria of desired workable air gaps and restricted acceleration amplitudes for a running maglev vehicle. Considering the seismic wave propagation nature of horizontal ground motion, the coupled equations of motion for maglev vehicle/guideway system are formulated using a dynamic interaction model of a single-span suspended beam carrying multiple moving maglev masses. Then the governing equations of motion for the suspended beam associated with all the controlled maglev masses are transformed into a set of generalized equations by Galerkin's method [21–23] and solved by the Newmark method [24] in the time domain. From the numerical results, although the inclusion of horizontal seismic ground motion may result in a significant amplification on both dynamic responses of the vehicle/guideway interaction system, the proposed hybrid controller has the ability to achieve the performance criteria of traveling safety and ride quality through continuous air gap monitoring and sustaining acceleration adjustment.

2. Formulation and mathematical model

Because of the trait of large levitation gaps, an EDS-repulsive system provides a more *flexible* suspension system in vertical vibration for a moving maglev vehicle than an EMS-attractive one. For this reason, the use of a secondary suspension system to mitigate the interaction response between the cabin and levitation frame will be excluded in this paper. Thus, this study will model a maglev train as a series of maglev masses and focus on the *vertical* response of the maglev masses traveling over a single-span suspended guideway (Fig. 1). Based on the *deflection theory* [12,13,18] that can take into account the additional cable tension of a suspended beam due to live loads, appreciable simplifications for the suspended guideway and maglev vehicles are outlined as follows: (1) the suspended guideway girder is modeled as a linear
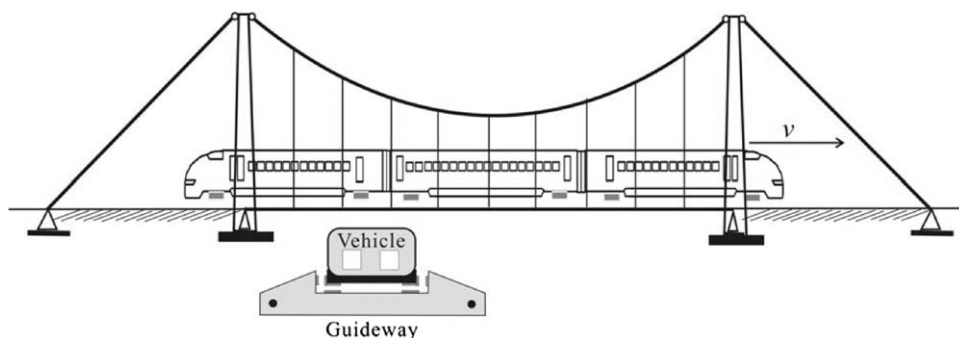

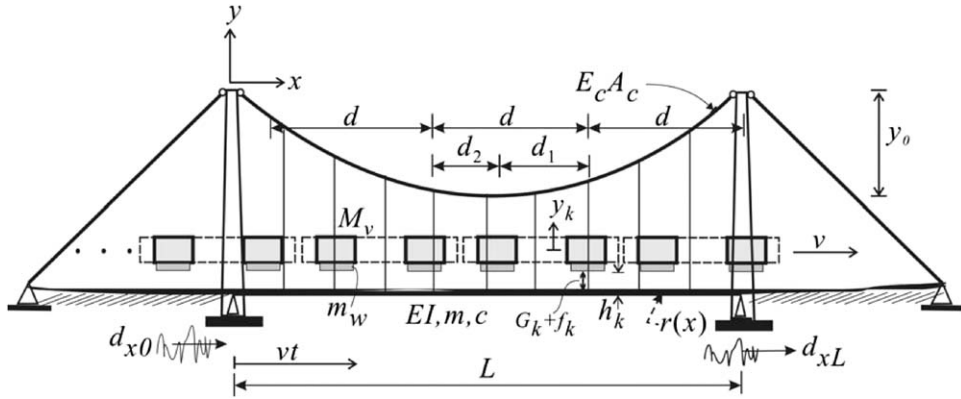**Fig. 1.** Suspended guideway traveled by a maglev train.

Fig. 2. Schematic diagram of multiple maglev masses running on a suspended beam shaken by horizontal earthquakes.

elastic Bernoulli–Euler beam with uniform cross section; (2) as shown in Fig. 2, the bridge towers are assumed so rigid that their deformations are negligible; (3) the suspension cable can carry all the dead loads of the stiffening girder with the aid of inextensible vertical hangers so that the suspended beam is in an un-stressed state before the action of live loads; (4) the maglev train passing over the suspended beam is simulated as a sequence of moving maglev masses with regular intervals; (5) only the horizontal ground motion in longitudinal direction along the guideway is considered; (6) there is no time delay between the input voltage and output current in the maglev suspension system.

2.1. Governing equations of a single-span suspended beam

For a parabolic cable under a uniform dead load w alone, the cable sag function $y(x)$ and the horizontal component T in the tensile cable can be respectively, expressed as [25]

$$y(x) = 4y_0[x/L - (x/L)^2],\tag{1}$$

$$T = \frac{-w}{y''} = \frac{wL^2}{8y_0},\tag{2}$$

where y_0=cable sag at mid-span and L=span length. Based on the *deflection theory* for small deformations of suspension bridges [12,13,17,18], the equation of vertical motion for a suspended beam carrying multiple moving maglev masses is given by:

$$m\ddot{u} + c\dot{u} + EIu'''' - (T + \Delta T)(y'' + u'') = w + p(x,t)$$

$$p(x,t) = -\sum_{k=1}^{K}[G_k(i_k, h_k) + f_k]\varphi(x,t),$$

$$\varphi(x,t) = \delta(x - x_k)[H(t - t_g - t_k) - H(t - t_g - t_k - L/v)],\tag{3}$$

where $(\cdot)' = \partial(\cdot)/\partial x$, $(\dot{\cdot}) = \partial(\cdot)/\partial t$, m=mass of the beam and cable per unit length along x-axis, c=damping coefficient, f_k=additional control force induced by a hybrid controller, G_k=control magnetic force, i_k=control current, h_k=levitation gap, $u(x,t)$=vertical deflection of the beam, EI=flexural rigidity of the beam, T=horizontal component in the initial cable tension (due to dead loads), ΔT=additional horizontal component in cable force due to external loads, $\delta(\cdot)$=Dirac's delta function, $H(t)$=unit step function, t_k=arrival time of the kth maglev mass into the beam, k=1, 2, 3,…, Kth moving maglev mass on the suspended beam, t_g=time lag for the first maglev mass entering the suspended beam, and $p(x,t)$=loading function of moving maglev masses. Consider the shaking effect of horizontal seismic support motion acting on the rigid bridge towers shown in Fig. 2, the time-dependent boundary conditions for the suspended beam with hinged ends are given by:

$$u_x(0,t) = d_{x0}(t), u_x(L,t) = d_{xL}(t),$$

$$u(0,t) = 0, u(L,t) = 0; EIu''(0,t) = EIu''(L,t) = 0,\tag{4}$$

where (d_{x0}, d_{xL}) represent the horizontal support movements at the left and right bridge towers, respectively. By including the horizontal support movements, an additional horizontal component ΔT in the cable due to external excitation is equal to [25]

$$\Delta T = \frac{E_c A_c}{L_c}\left[u_x|_0^L + \int_0^L y'u'\,dx\right] = \frac{E_c A_c}{L_c}\left[(d_{xL} - d_{x0}) + \frac{8y_0}{L^2}\int_0^L u\,dx\right],$$

$$L_c = \int_0^L \left(\frac{ds}{dx}\right)^3 dx = \int_0^L (\sqrt{1 + y'^2})^3\,dx,\tag{5}$$

in which E_c=elastic modulus of the cable, A_c=area of the cable, and L_c=the effective length of the cable. Substituting Eqs. (1), (2) and (5) into Eq. (3) yields the following equation of motion for a suspended beam under the simultaneous action of multiple moving maglev masses and horizontal support movements

$$m\ddot{u} + c\dot{u} + EIu'''' - (T + \Delta T_s)u'' + (\alpha + \kappa u'') \int_0^L u\, \mathrm{d}x = p(x,t) - \kappa(\mathrm{d}_{xL} - \mathrm{d}_{x0}), \quad (6)$$

where

$$\Delta T_s = \frac{E_c A_c}{L_c}(\mathrm{d}_{xL} - \mathrm{d}_{x0}),\, \alpha = \left(\frac{8y_0}{L^2}\right)^2 \frac{E_c A_c}{L_c},\, \kappa = \left(\frac{8y_0}{L^2}\right)\frac{E_c A_c}{L_c}. \quad (7)$$

As shown in Eq. (6), the horizontal ground motion may affect the vertical vibration of a suspended beam through multiple support movements, that is, $\mathrm{d}_{x0} \neq \mathrm{d}_{xL}$. Since the increment of horizontal component of cable force in Eq. (5) is dependent on both the beam deflection $u(x,t)$ and horizontal support movements (d_{x0}, d_{xL}), the integro-differential equation of motion in Eq. (6) is nonlinear in nature because of the presence of ΔT_s. Besides, an observation of Eq. (6) indicates that the approximation of $\alpha + \kappa u'' = \kappa(8y_0/L^2 + u'') \simeq \alpha$ is acceptable for the deflection theory of small amplitude, i.e., $|u''| \ll |y''| = 8y_0/L^2$.

2.2. Equation of a controlled maglev mass

As shown in Fig. 2, a series of maglev masses supported by repulsive-type magnetic forces are crossing a single-span suspended beam at constant speed. The governing equation of motion for the kth maglev mass is [3]

$$M\ddot{y}_k = -p_0 + G_k(i_k, h_k) + f_k, \quad (8)$$

where y_k=vertical displacement of the kth maglev mass.

From Lenz's law [33], as a magnet *passes over* a conductor, current will be induced in the conductor. As a result, a magnetic force component is created to act on the current-carrying conductor. This is so called the Lorentz force law [34]. Based on this concept, a magnetic force to levitate a vehicle is generated by the changing magnetic field (produced by the on-board magnets mounted on the vehicle) as well as the induced current (in a conducting guideway) once the running speed of a repulsive-type EDS maglev vehicle reaches a liftoff speed of about 100–120 km/h. In this study, the induced levitation force is designed to be linearly proportional to the tuning parameter of $(i_k/h_k)^2$ if the speed of the maglev vehicle exceeds the liftoff speed. Such an expression is to reflect the fact that the magnetic force increases as the levitation gap decreases during maglev vehicle/guideway interactions. Thus the repulsive levitation force to lift up the kth maglev mass can be represented by

$$G_k(i_k, h_k) = K_0 \times \left(\frac{i_k(t)}{h_k(t)}\right)^2, \quad (9)$$

where K_0=coupling factor, $i_k(t)=i_0+\iota_k(t)$=control current, $\iota_k(t)$=deviation of control current, $h_k(t) = h_0 + y_k(t) - u(x_k,t) + r(x_k)$=levitation gap, $r(x)$=irregularity of guideway, x_k=position of the kth maglev mass on the guideway, and (i_0, h_0)=desired control current and levitation gap around a specified nominal operating point for a maglev mass at static equilibrium. From the levitation force expressed in Eq. (9), its *motion-dependent* nature governs the interaction behavior of the maglev vehicle/guideway coupling system. Besides, one can obtain the suspension force to support the weight of the maglev mass at the desired control current and levitation gap of (i_0, h_0) from Eq. (9) as follows:

$$G_k(i_0, h_0) = \kappa_0(i_0/h_0)^2 = (M_v + m_w)g = Mg = p_0, \quad (10)$$

from which the coupling factor $\kappa_0 = p_0(h_0/i_0)^2$, g = gravity acceleration, and p_0=static weight of the lumped maglev mass $M = (M_v + m_w)$.

3. Design of a hybrid LQR+PID controller in conjunction with constraint rules

To keep up the operating performance of essential running safety and good ride quality for a maglev transport system, a maglev vehicle will be equipped with a proper controller that supplies necessary regulation of control efforts to the maglev suspension system. In this section, a hybrid controller that combines LQR (linear quadratic regulator) optimal algorithm for control actuator, PID (proportional, integral, derivative) tuning method for regulating control voltage, and constraint rule base for achieving the operating performance of a moving maglev vehicle will be carried out in the following.

3.1. LQR optimal controller

Based on the minimization of a given control performance index, LQR algorithm has been widely used in optimal control for its simplicity, reliability, robustness, and stability in a closed-loop system [26]. For the purpose of illustration, the feedback tuning gain to control the dynamic response of the kth maglev mass using LQR optimal algorithm is denoted as g_k

and Eq. (8) is rewritten as

$$M\ddot{y}_k = -p_0 + G_k(i_k, h_k) + g_k, \tag{11}$$

By introducing the state space as $\langle z_k \rangle = \langle y_k \ \dot{y}_k \rangle$, Eq. (11) can be transformed into a set of first order differential equations in the following matrix form [26]

$$\{\dot{z}_k\} = [A]\{z_k\} + \{B\}g_k + \{C\}(G_k - p_0), \tag{12}$$

$$[A] = \begin{bmatrix} 0 & 1 \\ 0 & 0 \end{bmatrix}, \{B\} = \begin{Bmatrix} 0 \\ 1/M \end{Bmatrix}, \{C\} = \begin{Bmatrix} 0 \\ 1/M \end{Bmatrix}, g_k = [G]\{z_k\}, \tag{13}$$

where $\{z_k\} = \langle z_k \rangle^{\mathrm{T}}$ and $[G]$ represents the control gain matrix. In this control algorithm, the control gain g_k is determined by minimizing the following quadratic cost index [26]

$$J_k = \int_0^{t_f} [\{z_k\}^{\mathrm{T}}[Q]\{z_k\} + Rg_k^2]\,\mathrm{d}t. \tag{14}$$

Here, $[Q]$ is a symmetric positive semi-definite weighting matrix for the performance of a structural system and R the weighting parameter for the input control force. The physical interpretation of Eq. (14) is that $\{z_k\}^{\mathrm{T}}[Q]\{z_k\}/2$ can be regarded as the sum of strain energy and kinetic energy in the system, and Rg_k^2 as the control energy through the tuning actuator. To minimize the performance index J_k in Eq. (14), the Riccati equation [26] is usually used to obtain the Riccati matrix $[P]$ and the control gain matrix $[G]$, i.e.,

$$[P][A] - \tfrac{1}{2}[P]\{B\}R^{-1}\{B\}^{\mathrm{T}}[P] + [A]^{\mathrm{T}}[P] + 2[Q] = [0], \tag{15}$$

$$[G] = -\tfrac{1}{2}R^{-1}[B]^{\mathrm{T}}[P]. \tag{16}$$

In this study, the weighting matrix $[Q]$ is represented by a diagonal matrix as

$$[Q] = \begin{bmatrix} k_b & 0 \\ 0 & M \end{bmatrix}. \tag{17}$$

Thus substituting Eqs. (13) and (17) into Eq. (15) gives the following solution of the Riccati matrix $[P]$:

$$[P] = 2M \begin{bmatrix} \sqrt{k_b(1 + \sqrt{Rk_b})/M} & \sqrt{k_bR} \\ \sqrt{k_bR} & \sqrt{2RM(1 + \sqrt{k_bR})} \end{bmatrix}, \tag{18}$$

and the corresponding control levitation force g_k at the kth magnets in Eq. (11) is equal to

$$g_k = [G]\{z_k\} = -\rho_1 y_k - \rho_2 \dot{y}_k$$

$$\rho_1 = \sqrt{k_b/R}, \rho_2 = \sqrt{M\left(2\sqrt{k_b/R} + \frac{1}{R}\right)}. \tag{19}$$

Finally, introducing the control force g_k of Eq. (19) into Eq. (11) gives the optimal control equation of the maglev mass using LQR control algorithm:

$$M\ddot{y}_k + \rho_2 \dot{y}_k + \rho_1 y_k = G_k(i_k, h_k) - p_0, \tag{20}$$

Observing the term $1/R$ in Eq. (19), it indicates that if R approaches to a very large value, i.e., $1/R \to 0$, Eq. (20) is reduced to the initial equation of motion with less input control gains to the controlled maglev mass. Moreover, the designer may select a pair of suitable stiffness and damping coefficients to reduce the vehicle's response to various degrees by trying different combinations of weighting parameters (k_b, R).

3.2. PID tuning regulator

As indicated earlier in Eq. (9), the magnetic levitation force is related to both the control current $i_k(t)$ and air gap $h_k(t)$. The voltage equation of control current for the kth maglev system is [3,10,11]

$$\Gamma_0 \frac{\mathrm{d}(i_k/h_k)}{\mathrm{d}t} + R_0 i_k = V_k, \tag{21}$$

where $\Gamma_0 = 2\kappa_0 =$ initial inductance of the coil winding the suspension magnet, $R_0 =$ resistance of the circuit, and $V_k =$ control voltage. To ensure the sustaining suspension function for the EDS-repulsive system, the PID tuning law [27,28] is applied to

regulating the control voltage, that is,

$$V_k = K_d \dot{e}_k + K_p e_k + K_i \int_0^t e_k \, \mathrm{d}t, \tag{22}$$

where K_d=derivative gain, K_p=proportional gain, and K_i=integral gain. Concerning the performance of PID parameters (K_p, K_i, K_d) in process control, a detailed interpretation for the tuning function of proportional, integral, and derivative is available in Refs. [27,28]. Let us adopt the variable transformation as $\gamma_k = i_k/h_k$, and the error function as $e_k = i_0/h_0 - i_k/h_k = \gamma_0 - \gamma_k$ in the control process. Then substituting Eq. (22) into Eq. (21) and differentiating this equation with respect to time, after some mathematical manipulation, one can achieve the following differential equation in terms of control error function

$$(\Gamma_0 + K_d)\ddot{e}_k + (K_p + R_0 h_k)\dot{e}_k + (K_i + R_0 \dot{h}_k)e_k - R_0\gamma_0\dot{y}_k = -R_0\gamma_0(\dot{u} - \dot{r})|_{x=x_k}. \tag{23}$$

With the aid of control error function e_k and $\gamma_0 = i_0/h_0$ defined previously, the combination of Eqs. (20) and (23) yields the following equations of motion for the kth maglev mass equipped with an on-board hybrid LQR+PID controller

$$[m_{v,k}]\{\ddot{u}_{v,k}\} + [c_{v,k}]\{\dot{u}_{v,k}\} + [k_{v,k}]\{u_{v,k}\} = \{f_{v,k}\}, \tag{24}$$

of which the displacement vector $\{u_{v,k}\}$, force vector $\{f_{v,k}\}$, and structural matrices of $[k_{v,k}]$, $[c_{v,k}]$, and $[m_{v,k}]$ are given as follows:

$$[m_{v,k}] = \begin{bmatrix} M & 0 \\ 0 & K_d + \Gamma_0 \end{bmatrix}, \quad [c_{v,k}] = \begin{bmatrix} \rho_2 & 0 \\ -R_0\gamma_0 & K_p + R_0 h_k \end{bmatrix},$$

$$[k_{v,k}] = \begin{bmatrix} \rho_1 & 2p_0/\gamma_0 \\ 0 & K_i + R_0\dot{h}_k \end{bmatrix}, \{f_{v,k}\} = \left\{ \begin{array}{c} p_0 \times e_k^2/\gamma_0^2 \\ -R_0\gamma_0(\dot{u} - \dot{r})|_{x=x_k} \end{array} \right\}, \{u_{v,k}\} = \left\{ \begin{array}{c} y_k \\ e_k \end{array} \right\}. \tag{25}$$

3.3. Constraint rule base for operating performance

To achieve a better operating performance of maglev transport system, the dynamic response of the moving maglev vehicle plays a key role in determining the ride quality measured by acceleration response ($\ddot{y}_k$) and the running safety detected by working air gap (h_k). For this reason, they have to be limited to a workable range. For example, the oscillating amplitude of magnets should be bounded by a limited range of air gaps ε_k and the allowable maximum acceleration amplitude $|\ddot{y}_k|$ of vehicle's response is also limited to an upper bound of $a_{\max}$. To meet these performance criteria, the following constraint conditions that force the responses of the moving maglev masses to achieve operating performance for a working maglev system are required:

$$|\ddot{y}_k| \le a_{\max}, \varepsilon_k = \begin{cases} h_{\min} & h_k \le h_{\min} \\ h_{\max} & h_k \ge h_{\max} \end{cases}. \tag{26a,b}$$

Here, ($h_{\min}$, $h_{\max}$) are denoted as the lower and upper bounds of working air gap, respectively. According to the responses of ($h_k, \ddot{y}_k$) measured from a moving maglev mass, a constraint rule base loaded for the performance criteria is summed up as follows:

$$\text{Rule 1}: \text{ if } (h_{\min} < h_k < h_{\max}) \quad \text{and} \quad |\ddot{y}_k| \le a_{\max} \text{ then } [\![\, h_k, \ddot{y}_k \,]\!]; \tag{27a}$$

$$\text{Rule 2}: \text{ if } (h_k \ge h_{\max} \text{ or } h_k \le h_{\min}) \quad \text{and} \quad |\ddot{y}_k| \le a_{\max} \text{ then } [\![\, h_k = \varepsilon_k, \ddot{y}_k \,]\!]; \tag{27b}$$

$$\text{Rule 3}: \text{ if } (h_{\min} < h_k < h_{\max}) \quad \text{and} \quad \ddot{y}_k \ge a_{\max} \text{ then } [\![\, h_k, \ddot{y}_k = \text{sgn}(\ddot{y}_k) \times a_{\max} \,]\!]; \tag{27c}$$

$$\text{Rule 4}: \text{ if } (h_k \ge h_{\max} \text{ or } h_k \le h_{\min}) \quad \text{and} \quad |\ddot{y}_k| \ge a_{\max} \text{ then } [\![\, h_k = \varepsilon_k, \ddot{y}_k = \text{sgn}(\ddot{y}_k) \times a_{\max} \,]\!]. \tag{27d}$$

Here, $[\![\cdot]\!]$ means an activation function for the constraint conditions included to work, and the sign function of $\text{sgn}(\cdot)$ is defined as

$$\text{sgn}(\ddot{y}_k) = \begin{cases} 1 & \ddot{y}_k > 0 \\ -1 & \ddot{y}_k < 0 \end{cases} \tag{28}$$

As shown in the constraint conditions of Eq. (27), the Rule 1 means the normal operating case of a moving maglev mass, and the Rules 2–4 represent the constraint conditions need to be activated due to excessive vibrations detected from the maglev mass's response. In order to impose the constraint rules to the maglev mass system, by Hamilton's principle and the concept of Lagrangian multipliers [29], the variational equation of potential energy for the kth moving maglev mass is given by [29]

$$\int_{t_1}^{t_2} \delta[T_k - U_k] \, \mathrm{d}t + \int_{t_1}^{t_2} \delta W \, \mathrm{d}t = 0, \tag{29}$$

where T_k=kinetic energy of the maglev mass, U_k=potential energy, δW=virtual work done by control force, and

$$T_k = \tfrac{1}{2}M\ddot{y}_k^2, \tag{30}$$

$$U_k = \lambda_k(t) \times (h_k - \varepsilon_k) + \Lambda_k(t) \times (\ddot{y}_k - \ddot{y}_{\max} \times \operatorname{sgn}(\ddot{y}_k)), \tag{31}$$

$$\delta W = Q_k \delta y_k = (G_k(i_k, h_k) - p_0 + g_k) \times \delta y_k, \tag{32}$$

Here, λ_k and Λ_k represent the Lagrangian multipliers to restrict the response of $(h_k, \ddot{y}_k)$ within the limited range shown in Eq. (26). By applying the variational principle to Eq. (29) and admitting the arbitrary nature of $(\delta y_k, \delta\lambda_k, \delta\Lambda_k)$, the governing equations associated with the LQR+PID tuning algorithm as well as the constraint rule base listed in Eq. (27) are outlined as follows:

(1) Rule 1: if $(h_{\min} < h_k < h_{\max})$ and $|\ddot{y}_k| \le a_{\max}$ then

$$[m_{v,k}]\{\ddot{u}_{v,k}\} + [c_{v,k}]\{\dot{u}_{v,k}\} + [k_{v,k}]\{u_{v,k}\} = \{f_{v,k}\}, \tag{33a}$$

(2) Rule 2: if $(h_k \ge h_{\max} \text{ or } h_k \le h_{\min})$ and $|\ddot{y}_k| \le a_{\max}$ then

$$\begin{bmatrix} [m_{v,k}] & 0 \\ 0 & 0 \end{bmatrix}\left\{\begin{matrix} \{\ddot{u}_{v,k}\} \\ \ddot{\lambda}_k \end{matrix}\right\} + \begin{bmatrix} [c_{v,k}] & 0 \\ 0 & 0 \end{bmatrix}\left\{\begin{matrix} \{\dot{u}_{v,k}\} \\ \dot{\lambda}_k \end{matrix}\right\} + \begin{bmatrix} [k_{v,k}] & 1 \\ 1 & 0 \end{bmatrix}\left\{\begin{matrix} \{u_{v,k}\} \\ \lambda_k \end{matrix}\right\} = \begin{bmatrix} \{f_{v,k}\} \\ \varepsilon_k - (h_0 - u(x_k) + r(x_k)) \end{bmatrix}, \tag{33b}$$

(3) Rule 3: if $(h_{\min} < h_k < h_{\max})$ and $|\ddot{y}_k| \ge a_{\max}$ then

$$\begin{bmatrix} [m_{v,k}] & -1 \\ 1 & 0 \end{bmatrix}\left\{\begin{matrix} \{\ddot{u}_{v,k}\} \\ \ddot{\Lambda}_k \end{matrix}\right\} + \begin{bmatrix} [c_{v,k}] & 0 \\ 0 & 0 \end{bmatrix}\left\{\begin{matrix} \{\dot{u}_{v,k}\} \\ \dot{\Lambda}_k \end{matrix}\right\} + \begin{bmatrix} [k_{v,k}] & 0 \\ 0 & 0 \end{bmatrix}\left\{\begin{matrix} \{u_{v,k}\} \\ \Lambda_k \end{matrix}\right\} = \begin{bmatrix} \{f_{v,k}\} \\ a_{\max} \times \operatorname{sgn}(\ddot{y}_k) \end{bmatrix}, \tag{33c}$$

(4) Rule 4: if $(h_k \ge h_{\max} \text{ or } h_k \le h_{\min})$ and $|\ddot{y}_k| \ge a_{\max}$ then

$$\begin{bmatrix} [m_{v,k}] & 0 & -1 \\ 0 & 0 & 0 \\ 1 & 0 & 0 \end{bmatrix}\left\{\begin{matrix} \{\ddot{u}_{v,k}\} \\ \ddot{\lambda}_k \\ \ddot{\Lambda}_k \end{matrix}\right\} + \begin{bmatrix} [c_{v,k}] & 0 & 0 \\ 0 & 0 & 0 \\ 1 & 0 & 0 \end{bmatrix}\left\{\begin{matrix} \{\ddot{u}_{v,k}\} \\ \dot{\lambda}_k \\ \dot{\Lambda}_k \end{matrix}\right\} + \begin{bmatrix} [k_{v,k}] & 1 & 0 \\ 1 & 0 & 0 \\ 0 & 0 & 0 \end{bmatrix}\left\{\begin{matrix} \{u_{v,k}\} \\ \lambda_k \\ \Lambda_k \end{matrix}\right\}$$
$$= \left\{\begin{matrix} \{f_{v,k}\} \\ \varepsilon_k - (h_0 + u(x_k) + r(x_k)) \\ a_{\max} \times \operatorname{sgn}(\ddot{y}_k) \end{matrix}\right\}, \tag{33d}$$

Rule 1 represents that the responses of both air gap and acceleration of a maglev mass are within a workable range without constrains, but the case of Rule 4 is that the responses $(h_k, \ddot{y}_k)$ must be restricted due to intensive oscillation in the maglev mass system. With the present control strategy shown in Eqs. (33), an additional control force f_k required for regulating the dynamic response of the kth maglev mass is determined by

$$f_k = -(g_k + \lambda_k - \ddot{\Lambda}_k), \tag{34}$$

in which the Lagrangian multipliers of (λ_k, Λ_k) are obtained from the solution of Eqs. (33).

4. Solution by Galerkin's method

According to the homogeneous boundary conditions shown in Eq. (4), the dynamic deflection of the suspended beam can be approximated by [21–23]:

$$u(x,t) = \sum_{n=1} q_n(t) \sin\frac{n\pi x}{L}, \tag{35}$$

where $q_n(t)$ means the generalized coordinate associated with the nth assumed mode of the suspended beam. By Galerkin's method [12], one can transform the equation of motion for the suspended beam in Eq. (3) into the following generalized system equations [21–23]. Then, the nth generalized equation of motion of the suspended beam is:

$$m\ddot{q}_n + c\dot{q}_n + \left(\frac{n\pi}{L}\right)^2\left[\left(\frac{n\pi}{L}\right)^2 EI + (T + \Delta T_s)\right]q_n + \Pi_n = p_n(t) - \frac{2\kappa}{n\pi}(1 - \cos(n\pi))(\mathrm{d}_{xL} - \mathrm{d}_{x0}), \tag{36}$$

where

$$\Pi_n = \frac{2\alpha L}{n\pi^2}(1 - \cos n\pi)\left[\sum_{k=1}\frac{1}{k}(1 - \cos k\pi)q_k\right], \qquad (37)$$

$$p_n(t) = -\frac{2}{L}\sum_{k=1}^{K}[(G_k(i_k, h_k) + f_k) \times \psi_{jn}(\varpi_n, t)], \qquad (38)$$

$$\psi_n(\varpi_n, t) = \sin \varpi_n(t - t_k)[H(t - t_g - t_k) - H(t - t_g - t_k - L/v)], \qquad (39)$$

with $\varpi_n = n\pi v/L$ [21–23]. It is noted that the generalized loading function $p_n(t)$ in Eq. (38) is related to the control levitation forces obtained from Section 3. For this reason, an iterative method has to be carried out for solving the dynamic response of the maglev mass/guideway coupling system.

5. Applications of incremental-iterative approach

Because of *motion-dependent* nature of levitation forces due to the presence of air gaps, the nonlinear interaction analysis of the maglev vehicle/guideway system needs to be solved by iterative method. The procedure of incremental-iterative dynamic analysis involves the three phases: *predictor, corrector,* and *equilibrium checking* [10,11,32]. Fig. 3 shows the flow chart to carry out the nonlinear interaction analysis of controlled maglev vehicles running on a suspended guideway shaken by horizontal ground motion. It is noted that the structure matrices in Eq. (36) as well as the vehicle's equation associated with the activation of control process shown in Eqs. (33) should be updated and surveyed at each iteration.

Due to the presence of levitation gap for a maglev system, the compatible condition of deformation between the magnet and guideway girder is no longer available in dynamic interaction analysis. For this reason, the convergent condition of removing unbalanced forces by iterative method is a better way in carrying out the interaction analysis of the maglev mass/guideway coupling system. Let us define the root mean square of all the sum of unbalanced forces as

$$\beta_{tol} = \left[\sum_{k=1\dots}(\Delta f_{vk,t+\Delta t}^{i-1})^2 + \sum_{n=1\dots}(\Delta p_{n,t+\Delta t}^{i-1})^2\right]^{1/2}, \qquad (40)$$
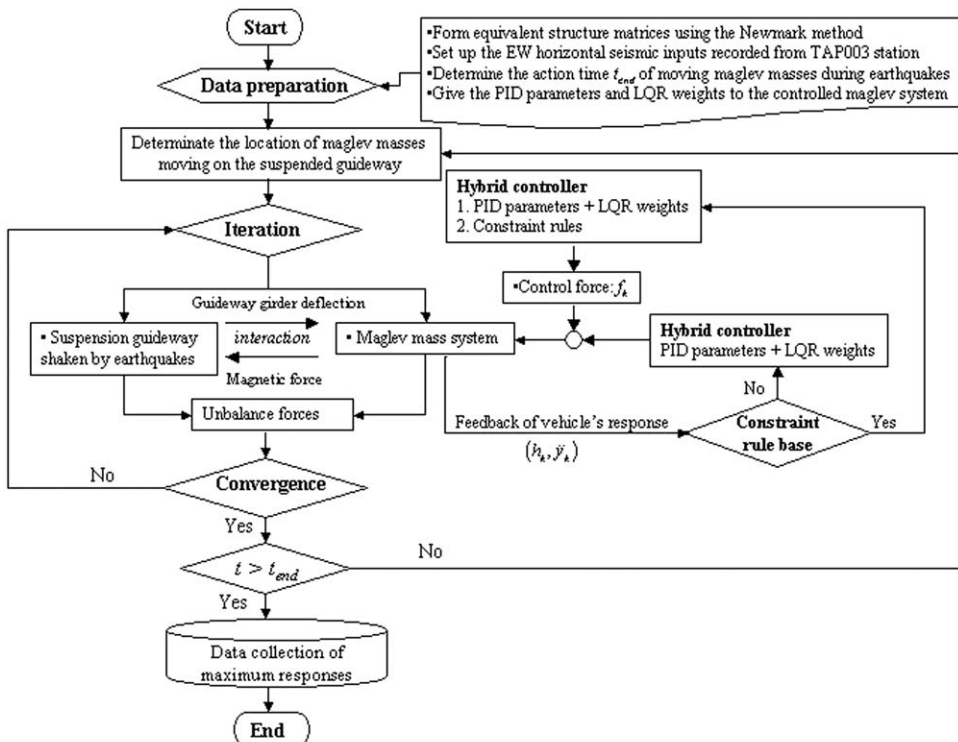

Fig. 3. Flow chart of incremental-iterative procedure with hybrid control process.

As β_{tol} is larger than a preset tolerance, say 10^{-3}, iteration for removing the unbalanced forces involving the predictor and corrector should be repeated (see the flow-chart in Fig. 3). Here, $\Delta p_{n,t+\Delta t}^{i-1}$=the unbalanced force between the external force $p_{n,t+\Delta t}^{i-1}$ and the effective internal forces $f_{n,t+\Delta t}^{i-1}$ for the nth generalized system resulting from the last iterative step at time $t+\Delta t$, and $\Delta f_{vk,t+\Delta t}^{i-1}$=the unbalanced force for the kth maglev mass. Details concerning the incremental-iterative procedure for dynamic analysis of vehicle/guideway interaction are available in Refs. [10,11,32].

6. Numerical investigations

To take into account the random nature and characteristics of track irregularity in a maglev system, the following *power spectrum density* (PSD) function for track class 6 designed by *Federal Railroad Administration* (USA) [13] is given to simulate the vertical profile of guide-rail geometry variations

$$S(\omega) = \frac{A_v \omega_c^2}{(\omega^2 + \omega_r^2)(\omega^2 + \omega_c^2)}$$

Here, ω=spatial frequency, A_v, (=1.5×10^{-7} m), ω_r (=2.06×10^{-6} rad/m), and ω_c (=0.825 rad/m) are relevant parameters. Fig. 4 shows the vertical profile of track irregularity for the simulation of guide-rail geometry variations in this study. In addition, the time step of 0.005 s is employed to compute the interaction responses of the maglev mass/guideway coupling system.

As the schematic diagram of Fig. 2, a series of moving maglev masses (4 cars simulated by 8 lumped masses) are crossing a single-span suspended beam at constant speed v. The properties of the suspended beam and maglev mass unit are listed in Tables 1 and 2, respectively. In Table 1, the symbol of f_i represents the ith modal frequency of the suspended
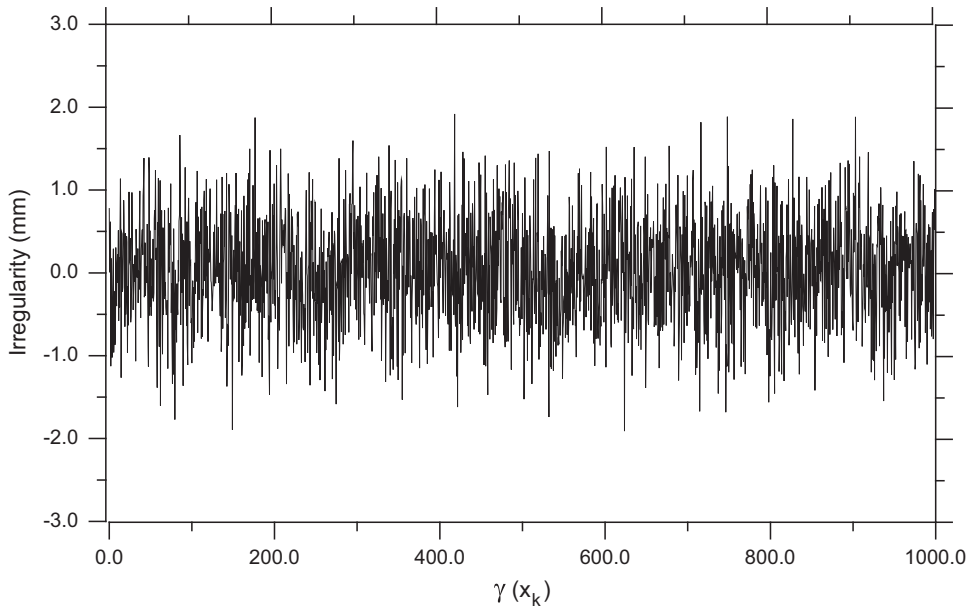

Fig. 4. Track irregularity (vertical profile).

Table 1
Properties and natural frequencies of the suspended beam.

L (m)	EI (kN m^2)	$E_c A_c$ (kN)	m (t/m)	c (kN s/m/m)	y_0 (m)	$E_c A_c / L_e$ (kN/m)	f_1 (Hz)	f_2 (Hz)
80	2.96×10^7	1.6×10^7	5	1.88	8.8	1.82×10^5	2.42	2.72

Table 2
Properties of moving oscillator and resonant speeds.

d (=d_1+d_2) (m)	d_1 (m)	d_2 (m)	M_v (t)	m_w (t)	i_0 (A)	R_0 (Ω)	$v_{res,1}$ (km/h)	$v_{res,2}$ (km/h)
25	20	5	18	2	25	1.0	218	245

beam. It is noted that the first natural frequency of anti-symmetric mode is lower than that one of symmetric bending mode due to the strengthening effect of cable tension [17]. Generally speaking, the acceleration response of vehicle-bridge system is usually used to evaluate the ride quality and maneuverability of high-speed ground transport system [21–23]. From the numerical results shown in Ref. [17], the use of first 16 modes is considered sufficient to compute the dynamic response of a suspended beam under the action of multiple moving loads. For this reason, the same number of modes will be used in all the examples to follow. Moreover, as the *passage frequency* ($=v/d$) of train loadings with regular interval (d) matches any of natural frequencies (f_i) of a bridge, the resonant response of the bridge will be developed [30,31], and the corresponding speed is denoted as $v_{res,i} = f_i d$ [21–23]. This is so called *resonance phenomenon* for train-induced response of railway bridges. In the following numerical examples, the levitation gap (h_k) of any of the moving maglev masses should be always positive for running safety.

6.1. Numerical verification

Prior to investigating the dynamic response of the maglev vehicle/guideway system subject to horizontal ground motion, a TR06 maglev vehicle model referred to as Ref. [9] is selected to simulate its dynamic behavior running on a single-span concrete guideway girder with *smooth* surface. Let us represent the TR06 maglev vehicle as 8 lumped maglev masses with identical intervals ($d_1=d_2=3$ m) moving at constant speed of 400 km/h [9]. The main data for the TR06 maglev vehicle model and the guideway girder [2,9] are given as follows: EI=24.56 × 10^6 kN m^2, L=24.854 m, m=3760 kg/m, M=7.6 t, h_0=8 mm, i_0=37 ampere (A), and R_0=1.1 ohm (Ω). Considering the PID parameters of (K_p=0.015, K_i=20, K_d=0.027), the time history responses of mid-span guideway deflection and the acceleration of the first maglev mass, together with the numerical results referred to as references [9,10], have been plotted in Figs. 5 and 6, respectively. They indicate that the proposed maglev vehicle/guideway model has the ability to simulate the dynamic behavior of a TR06 maglev vehicle running on a concrete guideway.

6.2. Determination of PID parameters based on Z–N tuning rules

In designing an LQR controller, one of the important issues is to determine its weighting parameters. Trying different combinations of weighting parameters (k_b,R) would be a suitable approach for designers to select a pair of stiffness and damping coefficients(ρ_1, ρ_2) in Eq. (20) to control the vehicle's response. In this example, the low natural frequency and high damping ratio (say, 2.3 rad/s and 0.87) [35] for the suspended maglev mass would be regarded as target parameters for the suspended maglev mass. Thus the LQR parameters as (k_b=100, R=0.01) are selected in Eqs. (19) and (20). With the same initial control voltage $R_0 i_0$ for the maglev suspension system, two desired levitation gaps, i.e., h_0=0.15 m/0.1 m, are respectively, used for the present maglev train model with four vehicles. They are named as MG-1 and MG-2, respectively. First, an on-board PID controller is employed to regulate the levitation force $G_k(i_k, h_k)$ in the EDS maglev system. From the textbooks in Refs [27,28], the Z–N tuning rule has been proved very useful in determining the optimal parameters of a PID controller for its simplicity, systematic procedure, and robustness in process control, from which the optimal PID
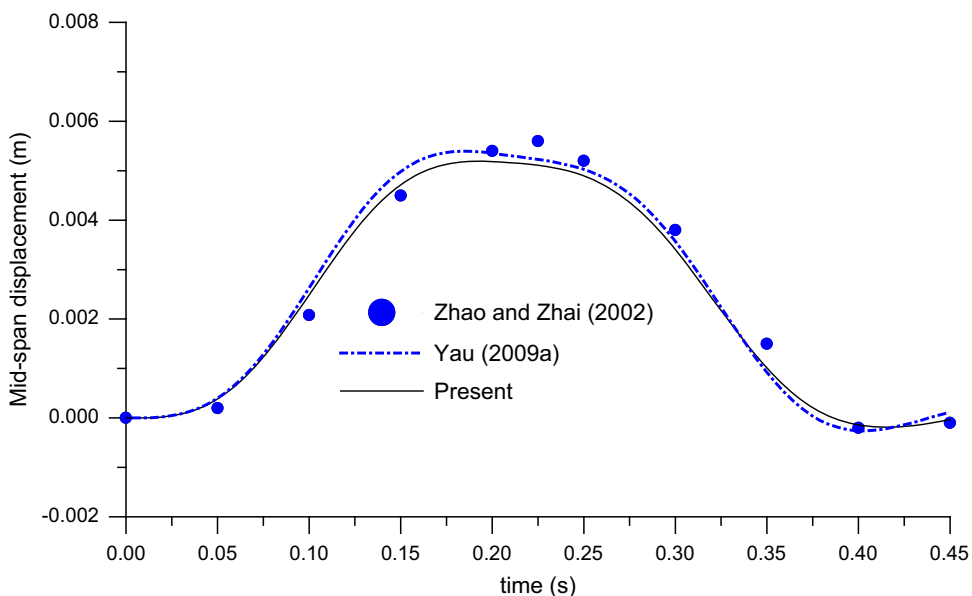

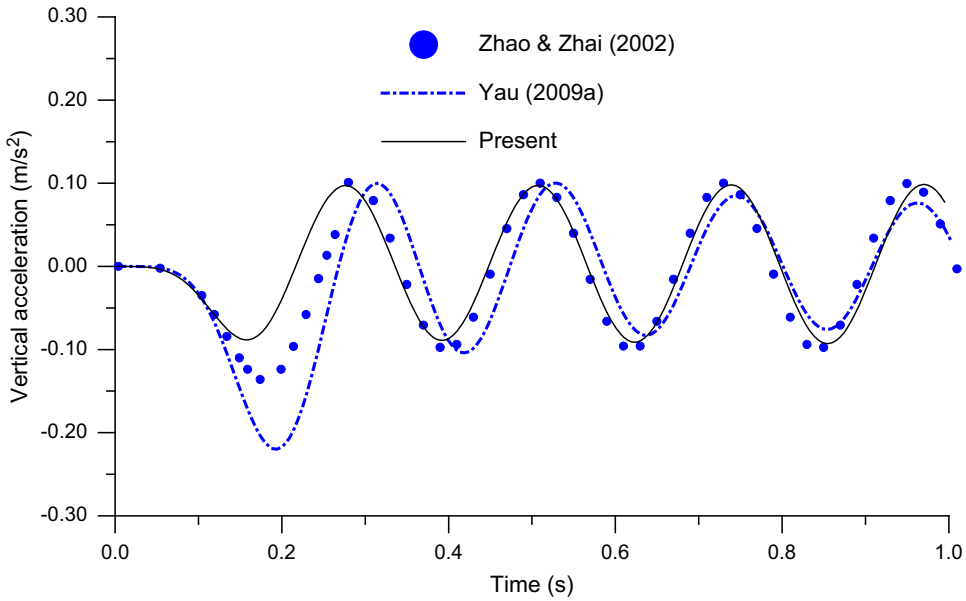**Fig. 5.** Time history response of mid-span displacement.

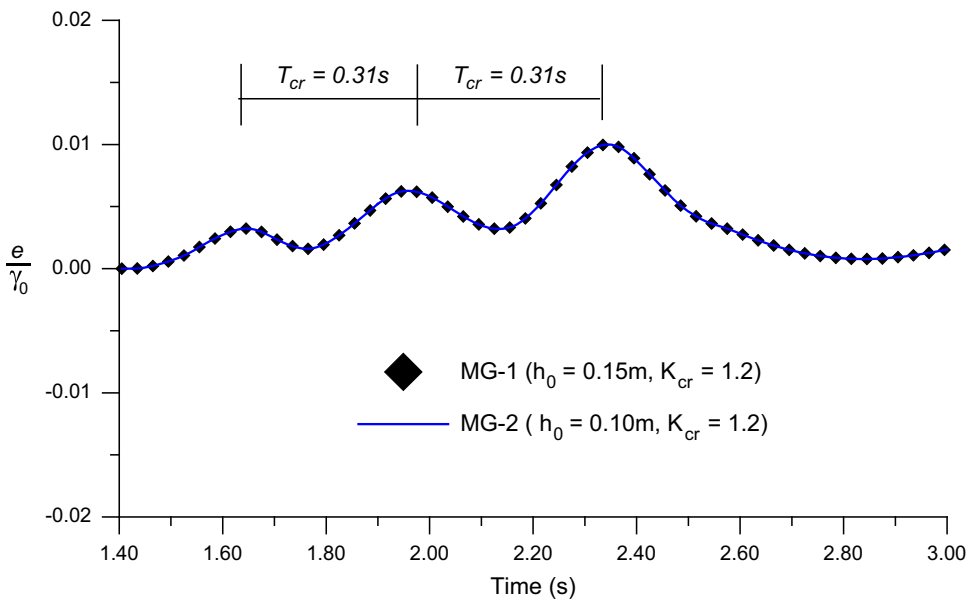**Fig. 6.** Time history response of vertical acceleration for maglev oscillator.

Fig. 7. Transient oscillation with a critical period T_{cr}.

parameters are given by $K_p=0.6K_{cr}$, $K_i=1.2K_{cr}/T_{cr}$, and $K_d=K_{cr}T_{cr}/8$. Here K_{cr} means the critical proportional gain of the PID controller by increasing only the proportional control action (i.e., $K_i=K_d=0$) K_p from 0 to a critical value K_{cr} so that the output first exhibits an oscillation behavior with a critical period T_{cr} [28].

To determine the optimal PID parameters based on Z–N tuning rules, the tuning parameters of K_i and K_d are first set to zero. Let us consider the case that the maglev mass systems cross the suspended guideway girder with the higher resonant speed of 245 km/h. By trials for different K_p to reach the critical parameter K_{cr}, the corresponding time history responses of the non-dimensional control error e/γ_0 and acceleration for the last maglev mass of both MG-1 and MG-2 have been plotted in Figs. 7 and 8, respectively. They show that the critical periods of the control error function and the transient responses of MG-1 and MG-2 are almost identical. One explanation for this is that their large levitation gaps allow for additional vertical motion of a moving EDS-type maglev mass. Table 3 gives the corresponding optimal PID parameters
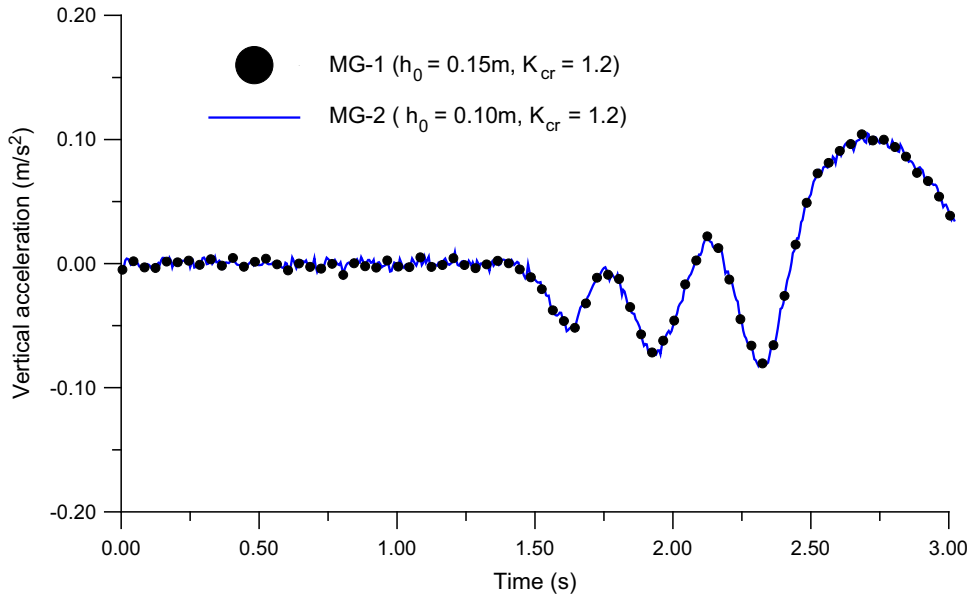
Fig. 8. Vertical acceleration of the last maglev mass.

Table 3
PID optimal parameters based on the Z–N tuning method.

Type	h_0 (m)	K_{cr}	T_{cr} (s)	K_p (=$0.6K_{cr}$)	K_i (=$1.2K_{cr}/T_{cr}$)	K_d (=$K_{cr}T_{cr}/8$)
MG-1/MG-2	0.15/0.10	1.2	0.31	0.72	4.65	0.047
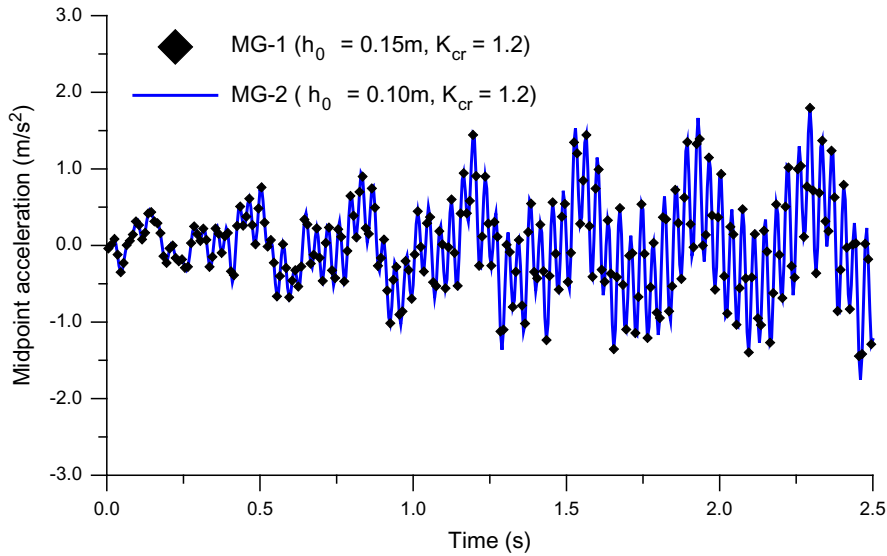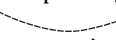
Fig. 9. Time history responses of midpoint acceleration of the suspended beam.

based on the Z–N tuning rules. It is noted that the time history response of acceleration in Fig. 8 for the last maglev mass is gradually built up due to the resonance phenomenon of the suspended beam mentioned earlier. Such a fact can be observed from Fig. 9, from which the time history response of midpoint acceleration of the suspended beam traveled by

MG-1 or MG-2 are identical in that the inertial forces induced by the moving maglev masses are much smaller than their static weights. This conclusion is consistent with that presented in Refs. [5,10].

6.3. Maximum acceleration response analysis

Let us use the optimal PID parameters listed in Table 3 to tune the control voltage of the maglev suspension system. By ranging the running speeds from 150–350 km/h with an increment of 5 km/h, the computed maximum acceleration responses ($a_{v,\max}$) of MG-1 and MG-2 against the speed (v) have been drawn in Fig. 10. Such a plot will be called $a_{v,\max}-v$ plot in the following examples. The numerical results indicate that the acceleration amplitude reaches its maximum value at the first resonant speed of 218 km/h but is suppressed at the second resonant speed of 245 km/h. One reason for this is that as a row of moving masses, with regular intervals of (d_1=20 m, d_2=5 m) far smaller than the guideway span (L=80 m), travel over a suspended beam, the simultaneous presence of multiple maglev masses on the guideway may produce a suppression action on the first symmetric bending mode (i.e., $\asymp\!\!\smile$), making the mid-span acceleration of the suspended guideway less severe compared with the first resonant case involving the anti-symmetric mode [17]. Such a
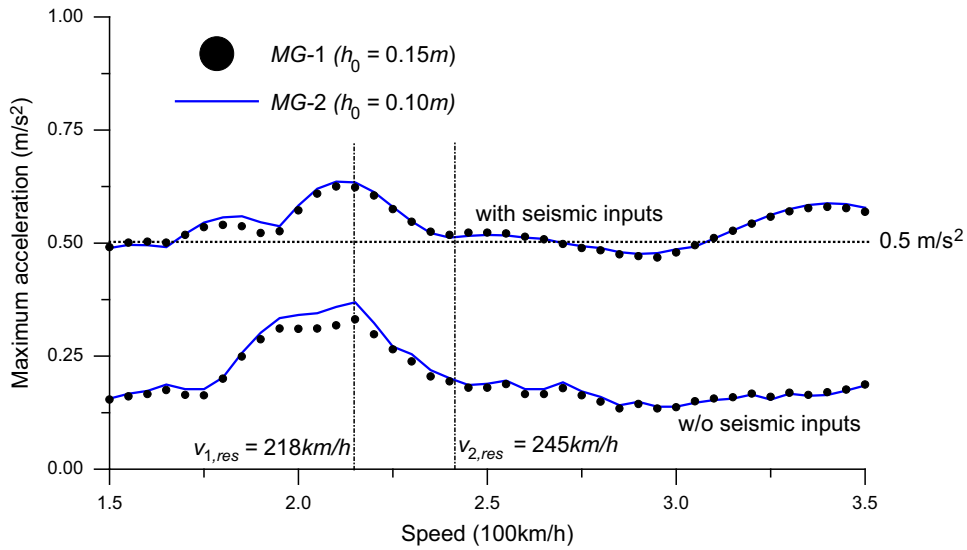

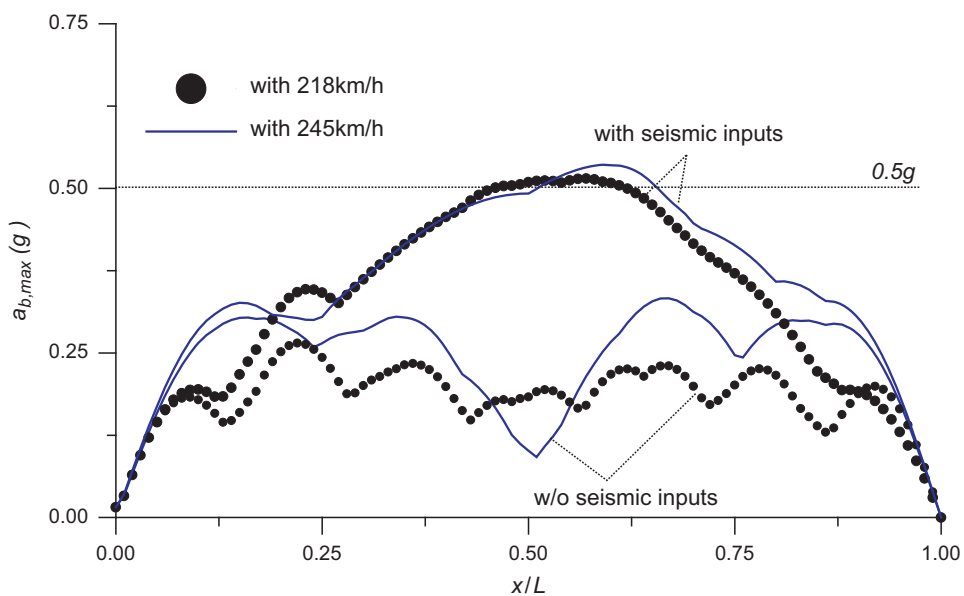**Fig. 10.** $a_{v,\max}-v$ plot for the maglev masses.

Fig. 11. Seismic effect on $a_{b,\max}-x/L$ plot.

phenomenon can be observed in the following illustration. Consider the maximum acceleration response amplitude ($a_{b,max}$) along the suspended beam (x/L) under the action of MG-1 and MG-2 moving with the first two resonant speeds, i.e., $v_{1,res}$ and $v_{2,res}$, respectively. The corresponding $a_{b,max}$–x/L plots have been drawn in Fig. 11. As can be seen from the resonant and sub-resonant peaks, the maximum acceleration response along the suspended beam with respect to the first two resonant speeds of 218 and 245 km/h are governed by the anti-symmetrical and symmetrical modes, respectively. But the mid-span acceleration amplitude of the beam is significantly suppressed at the second resonant speed of 245 km/h.

6.4. Effect of horizontal ground motion

To investigate the influence of seismic ground motion on interaction response of maglev vehicle/guideway system, the far-field ground motion recorded at free-field station (TAP003) during the 1999 Chi-Chi Earthquake in Taiwan [19] are used to simulate the seismic support inputs acting on the suspended guideway. The histogram of ground displacement containing the EW horizontal component has been plotted in Fig. 12. As can be seen, the intensive zone of horizontal ground movements appears nearby 25 s. In order to let the rear part of the maglev masses moving on the suspended guideway has the possibility to experience the action of peak ground motions in the duration between 25 and 28 s, the critical time of 25 s is employed for the maglev train model to start entering the guideway girder in the following examples. Besides, suppose the bridge foundations are anchored to bedrock in a rock site with a seismic wave speed of 1000 m/s and the ground motion at the right bridge support has a time lag of $L/1000$ (=0.08 s) behind the left one.

Consider the same vehicle/guideway model described in Example 6.3 and use the TAP003-EW seismic inputs shown in Fig. 12 to shake the suspended beam. The $a_{b,max}$–x/L plots with respect to the first two resonant speeds have been drawn in Fig. 11 as well, in which the maximum acceleration amplitudes are totally amplified and slightly greater than $0.5g$ (=4.9 m/s^2). Obviously, such excessive oscillations in the vibrating suspended beam will be a feedback to the maglev mass system over it. The corresponding $a_{v,max}$–v plots for MG-1 and MG-2 have been depicted in Fig. 10 as well. As can be seen from the $a_{v,max}$–v plots denoted by "with seismic inputs", the maximum acceleration amplitudes of the maglev masses are totally amplified due to seismic wave passage effect. Moreover, the upper/lower bounds of air gaps measured for MG-1 and MG2 to oscillate have been plotted in Figs. 13 and 14, respectively. The results indicate that either MG-1 (with larger air gap) or MG-2 requires more additional guideway clearance to allow for the excessive oscillations, especially for the case with seismic inputs. Considering the maximum control force defined as $F_{max}=(G_k-p_0+f_k)_{max}$ required for either MG-1 or MG-2, the maximum control efforts of F_{max}/p_0 against the moving speed (v) have been plotted in Fig. 15. As indicated from the F_{max}/p_0–v plots denoted by "w/o constraints", larger control efforts are used by the EDS maglev mass units to travel over the suspended guideway shaken by horizontal ground motion.

From the present study, the $a_{v,max}$–v plots with seismic inputs in Fig. 10 indicate that most of which have exceeded the upper bound of coded acceleration amplitude of $0.05g$ (=0.49 m/s^2) [5]. Besides, the vertical working air gap of the magnet motion in practice for a moving maglev vehicle should be restricted within a desired workable range. Because of this, the constraint rule base shown in Eqs. (33) will be applied to the hybrid LQR+PID controller in the following example.
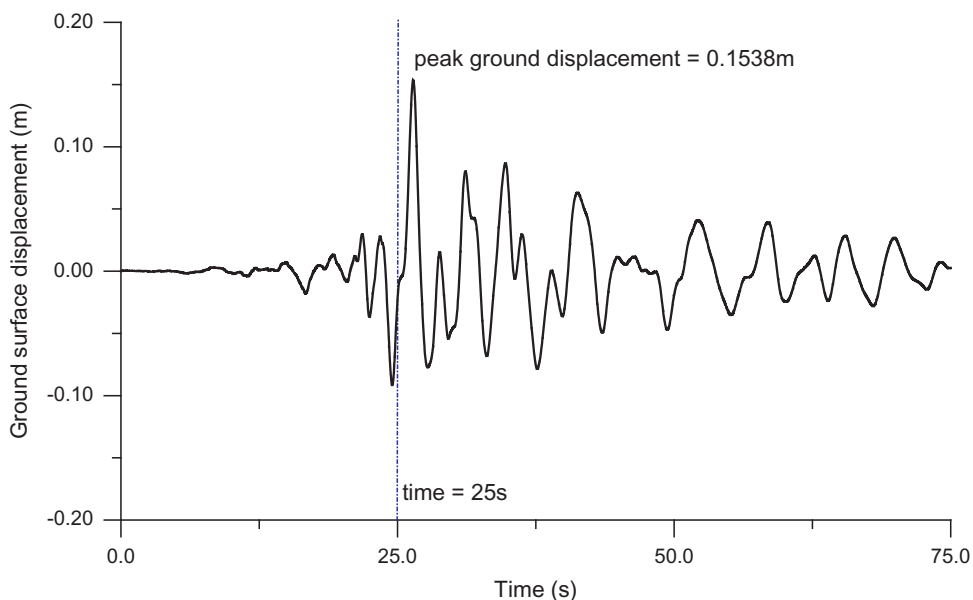

Fig. 12. Histogram of EW horizontal ground displacement of TAP003 Station.
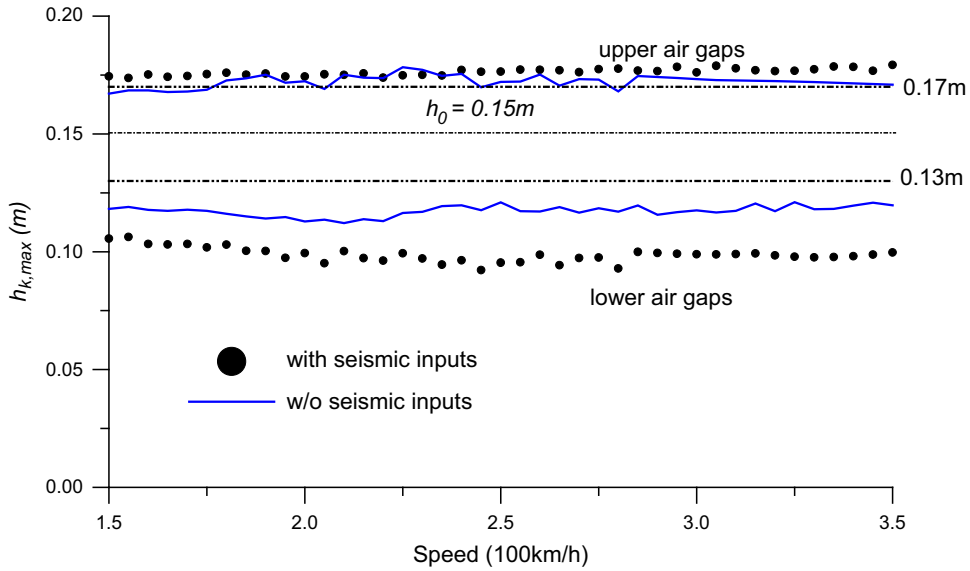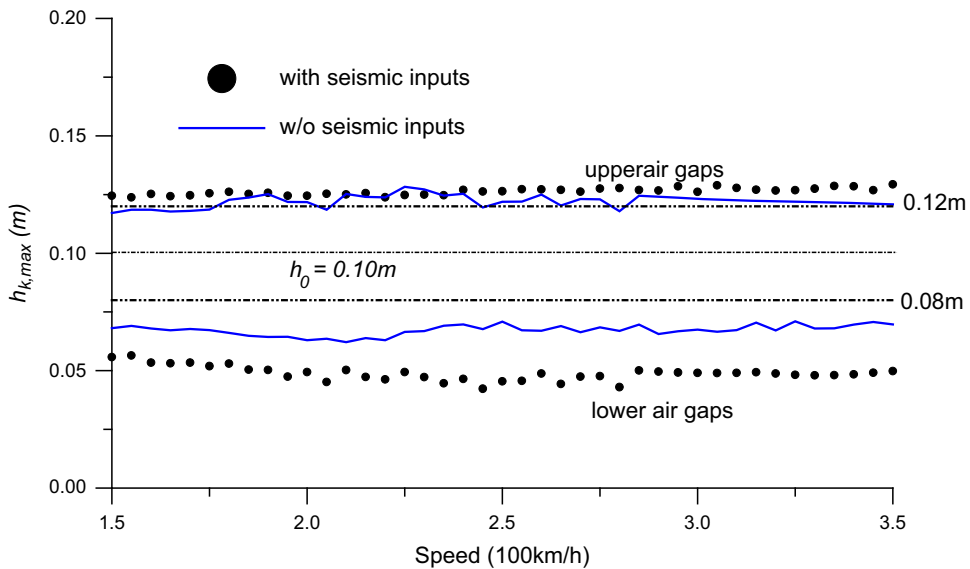
Fig. 13. Upper/lower air gaps of MG-1 (h_0=0.15 m).

Fig. 14. Upper/lower air gaps of MG-2 (h_0=0.10 m).

6.5. Applications of the hybrid controller with constraint rule base

For a maglev transport system, the dynamic response of a running maglev train provides important consequences for running safety and ride quality. The oscillating amplitude of magnet motion offers safety-related information and the acceleration response of maglev vehicles is concerned with ride quality of passenger cabins. According to the previous numerical investigations, the amplified levitation gap h_k due to the inclusion of earthquakes should be confined, that is, $h_{\min}(= h_0 - \Delta h) \le h_k \le h_{\max}(= h_0 + \Delta h)$. Here, Δh represents the oscillating amplitude of working air gap of the magnet motion. As for the upper and lower bounds of maximum vertical acceleration ($a_{\max}$) for the moving maglev masses, they are restricted to ± 0.5 m/s^2 [5]. For the purpose of illustration, let us consider the same case used in Section 6.4 and introduce the constraint values of ($a_{\max}$=0.5 m/s^2, Δh=0.02 m) to the constraint rule base shown in Eqs. (27). The upper bound of restricted acceleration ($a_{\max}$) and the limited range of levitation gaps have been depicted in Figs. 10, 13 and 14, respectively. Based on the control strategy shown in Eqs. (33), the $F_{\max}/p_0$–v plots of control efforts for MG-1 and MG-2
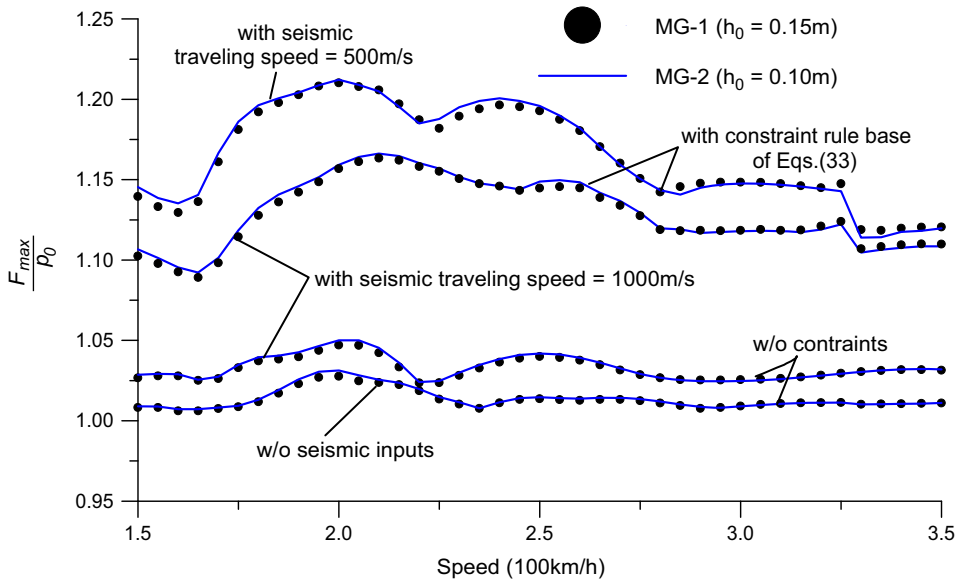
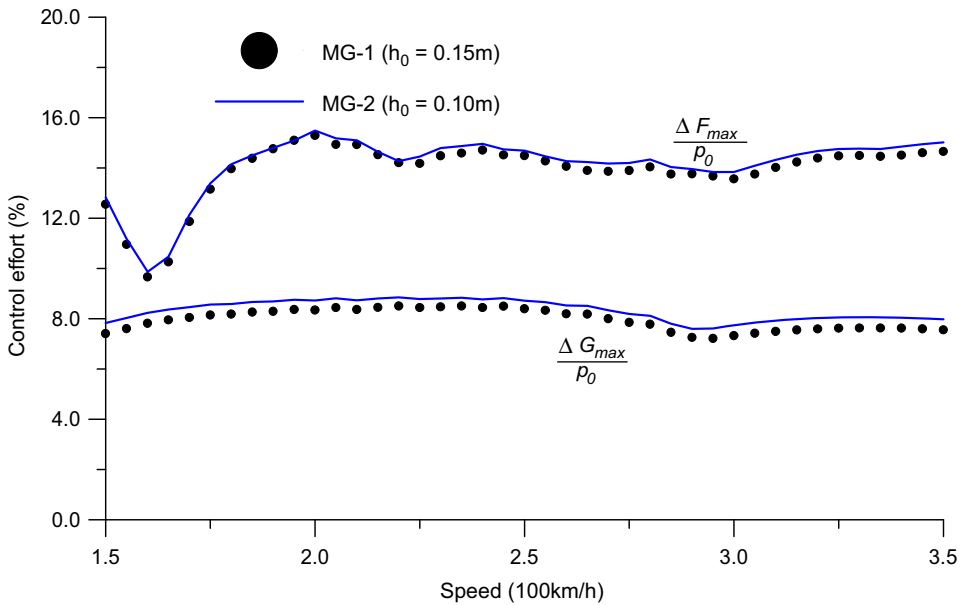**Fig. 15.** Maximum control efforts of controlled maglev mass units.

Fig. 16. Comparison of control efforts.

have been drawn in Fig. 15, respectively. As can be seen, the use of the proposed hybrid LQR+PID controller including constraint rule base has achieved the performance criteria required, but larger control gains are required to reach the predicted goals. Next, let us consider another case that the construction site of the suspended guideway locates at the region with a lower seismic wave speed of 500 m/s. Under the same constraint rule base described above, the corresponding F_{max}/p_0–v plots have been depicted in Fig. 15 as well. As can be seen for the cases with constraints, much larger control efforts are needed to keep up the performance requirements for the moving maglev vehicles. However, once the moving speed of the maglev masses exceeds the second resonant speed of 245 km/h, the increase of maximum control efforts decades rapidly. A possible explanation for this phenomenon is that the faster maglev train would experience less feedback excitations from the vibrating suspension guideway during earthquakes. Thus less control efforts are required for the fast maglev vehicles as well.

Meanwhile, let us consider the critical case of the construction site with traveling propagation velocity of 500 m/s. The control efforts required for the control actuator and the tuning equipment with control voltages have been plotted in Fig. 16, respectively. As shown in Fig. 16, $\Delta F_{max}/p_0 (= (f_k)_{max}/p_0)$ is denoted as the control effort induced by the control

actuator with constraint rules, and $\Delta G_{\max}/p_0 (= (G_k)_{\max}/p_0 - 1)$ by the regulating equipment with control voltage. The results show that the control actuator dominates most of the control efforts to satisfy the strict limitations of vertical response for levitation gap ($\Delta h = \pm 0.02$ m) and vehicle's acceleration response ($|\ddot{y}_{k,\max}| \leq 0.05$ g).

7. Concluding remarks

By using an incremental-iterative procedure in conjunction with control process, this paper has presented a computational framework of interaction analysis for a maglev train traveling over a suspension bridge shaken by horizontal ground motion. Concerning the running safety and ride quality of a moving maglev vehicle, an on-board hybrid LQR+PID controller with constraint rules is developed to control the dynamic response of the maglev vehicles. From the present study, the following conclusions are reached:

1. As the *passage frequencies* (v/d) caused by an EDS maglev train traveling over a suspended guideway girder coincides with any of the girder frequencies, resonance will be developed on the girder. Such a phenomenon has been observed from the $a_{b,\max}-x/L$ plots, in which higher modes are also excited.
2. The proposed hybrid LQR+PID controller provides a constraint rule base to adjust the working air gap within a prescribed stable region for traveling safety as well as to limit the maximum acceleration of ride quality for passengers.
3. Because of the trait of large air gaps, an EDS-type maglev vehicle offers enough guideway clearance to accommodate additional vertical motion of the magnets induced by earthquakes. Thus the dynamic responses of both the maglev mass systems, MG-1 (h_0=0.15 m) and MG-2 (h_0=0.1 m), are quite close.
4. The wave propagation effect induced by seismic ground motion plays a key role in affecting the interaction response of maglev vehicle/guideway system. The present investigation indicates that as a maglev train moves with lower traveling speeds, its controllers need to spend more control efforts achieving the operating performance desired for a maglev transport system.
5. In order to satisfy the strict performance requirements of vertical response for levitation gap ($\Delta h = \pm 0.02$ m) as well as vehicle's acceleration ($|\ddot{y}_{k,\max}| \leq 0.05$ g), from the present study, the control actuator with constraint rule base would dominate most of control efforts of the hybrid controller.
6. This study represents only parts of a preliminary attempt to simulate the vertical vibration behavior of a maglev train traveling a suspended bridge shaken by horizontal earthquakes. A further realistic model with 3D maglev vehicle should be carried out to investigate the influence of lateral seismic propagation on the dynamic stability of maglev train/ guideway interactions.

Acknowledgements

References

[1] D.L. Trumper, S.M. Olson, P.K. Subrahmanyan, Linearizing control of magnetic suspension systems, *IEEE Transactions on Control Systems Technology* 5 (4) (1997) 427–438.
[2] G. Bohn, G. Steinmetz, The electromagnetic levitation and guidance technology of the Transrapid test facility Emsland, *IEEE Transactions on Magnetics* 20 (5) (1984) 1666–1671.
[3] P.K. Sinha, *Electromagnetic Suspension, Dynamics and Control*, Peter Peregrinus Ltd., London, UK, 1987.
[4] A. Bittar, R.M. Sales, H_2 and H_∞ control for maglev vehicles, *IEEE Control Systems Magazine* 18 (4) (1998) 18–25.
[5] Y. Cai, S.S. Chen, D.M. Rote, H.T. Coffey, Vehicle/guideway dynamic interaction in maglev systems, *Journal of Dynamic Systems, Measurement, and Control* 118 (1996) 526–530.
[6] Y. Cai, S.S. Chen, Dynamic characteristics of magnetically-levitated vehicle systems, *Applied Mechanics Reviews* 50 (11) (1997) 647–670.
[7] X.J. Zheng, J.J. Wu, Y.H. Zhou, Numerical analyses on dynamic control of five-degree-of-freedom maglev vehicle moving on flexible guideways, *Journal of Sound and Vibration* 235 (2000) 43–61.
[8] X.J. Zheng, J.J. Wu, Y.H. Zhou, Effect of spring non-linearity on dynamic stability of a controlled maglev vehicle and its guideway system, *Journal of Sound and Vibration* 279 (2005) 201–215.
[9] C.F. Zhao, W.M. Zhai, Maglev vehicle/guideway vertical random response and ride quality, *Vehicle System Dynamics* 38 (3) (2002) 185–210.
[10] J.D. Yau, Vibration control of maglev vehicles traveling over a flexible guideway, *Journal of Sound and Vibration* 321 (2009) 184–200.
[11] J.D. Yau, Response of a maglev vehicle moving on a series of guideways with differential settlement, *Journal of Sound and Vibration* 234 (2009) 816–831.
[12] J.D. Yau, L. Fryba, Response of suspended beams due to moving loads and vertical seismic ground excitations, *Engineering Structures* 29 (2007) 3255–3262.
[13] L. Frýba, *Vibration of Solids and Structures Under Moving Loads*, third ed., Thomas Telford, London, 1999.
[14] J. Vellozzi, Vibration of suspension bridges under moving loads, *ASCE Journal of Structural Division* 93 (1967) 123–138.
[15] D. Bryja, P. Sniady, Spatially coupled vibrations of a suspension bridge under random highway traffic, *Earthquake Engineering & Structural Dynamics* 20 (1991) 999–1010.
[16] P.K. Chatterjee, T.K. Datta, C.S. Surana, Vibration of suspension bridges under vehicular movements, *ASCE Journal of Structural Division* 120 (1993) 681–703.
[17] J.D. Yau, Y.B. Yang, Vibration of a suspension bridge installed with a water pipeline and subjected to moving trains, *Engineering Structures* 30 (2008) 632–642.

[18] A. Pugsley, *The Theory of Suspension Bridges*, second ed., Edward Arnold Ltd., London, England, 1957.
[19] Y.B. Yang, J.D. Yau, Y.S. Wu, *Vehicle-Bridge Interaction Dynamics*, World Scientific, Singapore, 2004.
[20] H. Xia, Y. Han, N. Zhang, W. Guo, Dynamic analysis of train–bridge system subjected to non-uniform seismic excitations, *Earthquake Engineering & Structural Dynamics* 35 (2006) 1563–1579.
[21] J.D. Yau, Vibration of arch bridges due to moving loads and vertical ground motions, *Journal of Chinese Institute of Engineers* 29 (2006) 1017–1027.
[22] J.D. Yau, Vibration of parabolic tied-arch beams due to moving loads, *International Journal of Structural Stability and Dynamics* 6 (2006) 193–214.
[23] J.D. Yau, Train-induced vibration control of simple beams using string-type tuned mass dampers, *Journal of Mechanics* 23 (4) (2007) 329–340.
[24] N.M. Newmark, A method of computation for structural dynamics, *Journal of Engineering Mechanics Division* 85 (1959) 67–94.
[25] H.M. Irvine, *Cable Structures*, The MIT Press, Cambridge, 1981.
[26] T.T. Soong, *Active Structural Control: Theory and Practice*, Longman Scientific & Technical, Essex, England, 1990.
[27] K.J. Astrom, T. Hagglund, *Automatic Tuning of PID Controllers*, Instrument Society of America, North Carolina, 1988.
[28] K. Ogata, *Modern Control Engineering*, third ed., Prentice-Hall International Inc., Englewood Cliffs, NJ, 1997.
[29] R.W. Clough, J. Penzien, *Dynamics of Structures*, McGraw Hill, New York, 1975.
[30] Y.B. Yang, J.D. Yau, L.C. Hsu, Vibration of simple beams due to trains moving at high speeds, *Engineering Structures* 19 (1997) 936–944.
[31] J.D. Yau, Y.B. Yang, Vertical accelerations of simple beams due to successive loads traveling at resonant speeds, *Journal of Sound and Vibration* 289 (2006) 210–228.
[32] J.D. Yau, Response of a train moving on multi-span railway bridges undergoing ground settlement, *Engineering Structures* 31 (2009) 2115–2122.
[33] K.R. Davey, Electrodynamic maglev coil design and analysis, *IEEE Transactions on Magnetics* 33 (1997) 4227–4229.
[34] D.J. Griffiths, *Introduction to Electrodynamics*, third ed., Upper Saddle River, Prentice-Hall, NJ, 1999.
[35] A. Deepak, G. Fabrizio, Redesigning an active queue management system, *Proceeding of IEEE Communications Society GLOBECOM* (2004) 702–706.